

Reprinted from MONTHLY WEATHER REVIEW, Vol. 107, No. 9, September 1979  
American Meteorological Society  
Printed in U. S. A.

**Relationships between Large-Scale Motion and Convective Precipitation During GATE**

ROBERT W. REEVES AND CHESTER F. ROPELEWSKI

MICHAEL D. HUDLOW

## Relationships between Large-Scale Motion and Convective Precipitation During GATE

ROBERT W. REEVES AND CHESTER F. ROPELEWSKI

*Center for Environmental Assessment Services, Environmental Data and Information Service, NOAA, Washington, DC 20233*

MICHAEL D. HUDLOW

*Office of Hydrology, National Weather Service, NOAA, Washington, DC 20233*

(Manuscript received 14 November 1978, in final form 11 June 1979)

### ABSTRACT

Upper air and surface data from the GARP Atlantic Tropical Experiment (GATE) are used to examine the interrelationships between convective-scale precipitation and the larger scale wind field. The upper air winds from the inner (B) and outer (A/B) hexagonal observational arrays are fit with second-order polynomials to provide smooth estimates of the vorticity, divergence and vertical motion in the observational array. In these analyses we examined archived validated data from all three phases of the experiment and we formed averages based on the radar-estimated precipitation rates.

Mean profiles for 19-day periods during each of the three observational phases establish the basic similarity of the kinematics during each phase. Strong boundary-layer convergence balanced, for the most part, by upper tropospheric divergence, is common to all three phases.

Radar-estimated precipitation rates are used to define suppressed (precipitation rates  $<0.1 \text{ mm h}^{-1}$ ) and highly disturbed (precipitation rates  $>0.5 \text{ mm h}^{-1}$ ) states over the observational array. Mean profiles for the disturbed states in each phase show weaker easterly winds and much larger upward vertical velocities than do the mean profiles for the suppressed states. The mean vorticity profiles for each state do not show such clear-cut differences.

Time series of 12 h averages indicate that the precipitation events in Phase III corresponded very closely to the cyclonic maxima of the 700 mb relative vorticity, reflecting the influence of the easterly waves described by Reed *et al.* (1977). During Phases I and II, when easterly waves were poorly organized, the precipitation events did not correspond closely to the cyclonic vorticity maxima. On the other hand, precipitation events showed good correspondence with the large-scale (A/B) 700 mb upward vertical velocity maxima and surface meridional convergence  $\partial v/\partial y$  during all three phases. This shows that the precipitation is clearly related to events on a larger scale.

The effects of convective activity on the large-scale flow are examined through the vorticity budget. The vorticity budget residual profiles were similar from phase to phase with cyclonic production maxima in the mid and upper troposphere. The upper tropospheric residual maximum is as strong during the suppressed state as it is during the highly disturbed state. At the surface, individual values of the residual are almost always opposite in sign to the vorticity. The mean vorticity budget for the A/B array shows the tipping term to have magnitudes comparable to other terms in the vorticity budget.

### 1. Introduction

One of the primary aims of the GARP<sup>1</sup> Atlantic Tropical Experiment (GATE) was to gain an increased knowledge of the meteorology in the maritime tropics and its relation to the earth's general circulation. One of the specific goals was an understanding of tropical systems on various temporal and spatial scales, with emphasis on the interaction between the cumulus, cloud-cluster and synoptic scales (WMO GATE Rep. 1, 1972). The location of the experiment in the latitude band encompassing the convectively active Intertropical Convergence Zone (ITCZ) provided the data to study some aspects of these scale interactions. A number of re-

cent descriptive and quantitative studies utilizing GATE data have dealt with events on a particular scale and, to a limited extent, their interaction with events on other scales. Burpee (1975), using a compositing technique similar to that of Reed and Recker (1971), examined the mean flow characteristics of 24 synoptic-scale African waves using preliminary data from all three observation phases of GATE. He composited satellite data based on synoptic-scale wave phase, and found that maxima in the areal coverage of upper cloud coincided with maxima in the upward vertical motion. Reed *et al.* (1977) formed composites for the synoptic wave disturbances of the third observational phase. In addition to satellite images, they used precipitation estimates based on rain gauge measurements, and found a threefold increase in both satellite-inferred convective

<sup>1</sup> Global Atmospheric Research Program.

tive cloud and precipitation with passage of the wave trough. Thompson *et al.* (1979), using validated data from Phase III, which included radar precipitation estimates, performed a more extensive analysis of the composite easterly waves, and compared the waves of the eastern Atlantic and western Pacific. The presence of three distinct layers of divergence in the GATE wave led them to postulate the existence of three main cloud populations.

In an analysis of events on a smaller scale, Martin (1975) used satellite data to describe the characteristics of cloud clusters during GATE. Houze (1975) identified the principal squall lines which occurred during the experiment and used radar images to describe their behavior. In the range from cumulus to cloud-cluster scale, Houze and Cheng (1977) performed a statistical study on GATE radar echoes, relating individual echo lifetimes to horizontal and vertical dimensions. Their study confirmed the predominance of precipitation of convective origin.

The results of these studies suggest that the precipitation, while basically of convective origin, could be related to events on a larger scale, e.g., the troughs of synoptic-scale waves. Of fundamental interest then is whether the precipitation events can be related to kinematic quantities evaluated on scales much larger than individual convective elements. Related to this is the problem of determining the extent to which ensembles of convective elements affect the larger scale flow. We examine some aspects of this feedback through the study of the vorticity budget. Budget computations are performed for both suppressed and highly disturbed conditions.

The analysis is divided into four parts. In the first part, mean profiles of the divergence, vorticity and vertical velocity for each phase are presented. These means serve as the background required to discuss and interpret the results of the analyses presented in the following three parts. In part two, we form means for the suppressed and highly disturbed states and discuss similarities and differences. The relations between the larger scale winds in suppressed and enhanced states are examined in more detail in part three through the time series of precipitation, vorticity, divergence and vertical velocity. The effects of cumulus on the larger scale are discussed through the vorticity budget in part four.

**2. Data sources**

Rawinsonde and surface data taken by ships stationed in the inner (B-array) and outer (A/B array) hexagons of the GATE network (Fig. 1), provided the main sources of data for the computations used in this study. Precipitation rates were estimated from reflectivity data collected on four ships equipped with C-band digital radars. The analyses were per-

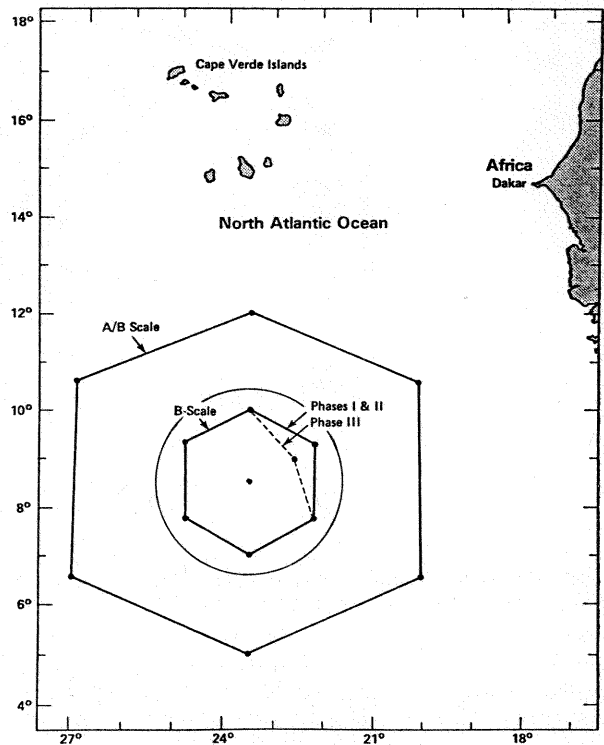


FIG. 1. GATE A/B and B ship arrays and the circular "master" array.

formed on three 19-day observation periods, one during each phase (Table 1).

Rawinsondes were launched at 3 h intervals during priority periods, e.g., periods of enhanced convection, and at 6 h intervals at other times. The archived validated upper air data set as described by Reeves (1978) was used for the computations. The data for all ships of the B and A/B arrays were used in a scheme which fit the zonal and meridional wind components to a quadratic surface. One advantage of this fitting scheme is that we may estimate the winds and their first derivatives anywhere in the array. The coefficients resulting from the least-squares-fitting scheme were then used to evaluate all of the kinematic quantities discussed below and the terms in the vorticity budget equation at the center of the arrays (8.5°N, 23.5°W). The data were fit in 25 mb layers and overlapping 12 h means every 6 h. The vorticity budget quantities have been averaged over 125 mb layers. Additional editing of the second-order coefficients was performed using the asymptotic singular decomposition technique of Jalickee and Klepczynski (1977).

TABLE 1. Periods of observation during GATE.

Phase I	28 June-16 July
Phase II	28 July-15 August
Phase III	30 August-17 September

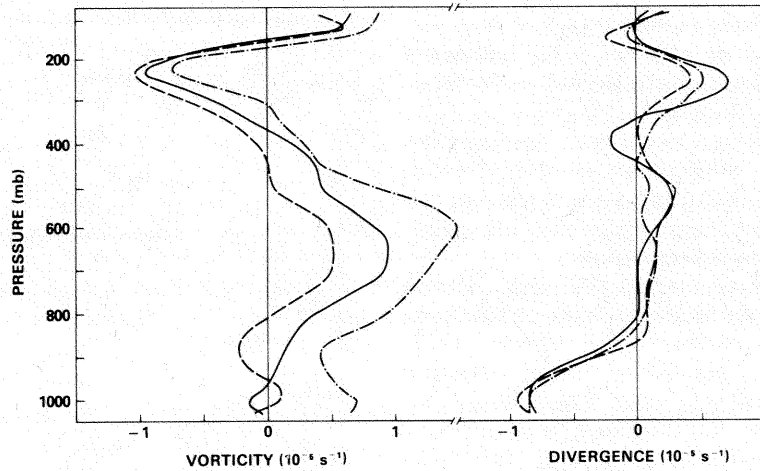


FIG. 2. Mean relative vorticity and divergence profiles. Phase I (dashed-dotted), Phase II (dashed) and Phase III (solid).

The vertical velocity was computed by vertical integration of the horizontal divergence, with mass balance insured at 100 mb utilizing a method (O'Brien, 1970) which assumes that errors in computed divergence increase linearly with decreasing pressure. This is a reasonable assumption for the errors associated with winds derived from the radar-tracked sondes of the outer hexagon. In the vorticity budget computations, which require horizontal gradients of vertical velocity, O'Brien's technique was also employed; i.e., the horizontal gradients were set equal to zero at 100 mb with adjustment at other levels a linear function of pressure.

The rainrates were estimated from the radar reflectivity data, which were verified by intership comparisons as well as with shipboard rain gauge calibrations (Hudlow *et al.*, 1979). The 12 h esti-

mated precipitation rates were formed by averaging four 3 h rates over the B array or the "master" array as described by Hudlow and Patterson (1979). The master array covered a circular area extending approximately 200 km in radius, i.e., slightly larger than the B-array. Averages over the B array were used except for the comparison of B- and A/B-array vertical velocities with rainfall. In this case the average rainrate over the master array was used for the comparison over the A/B array. Data from the individual radars were merged to obtain the refined precipitation estimates over the B and master arrays.

### 3. Analyses

Means for each phase, for the wind components and their spatial derivatives and for the derived

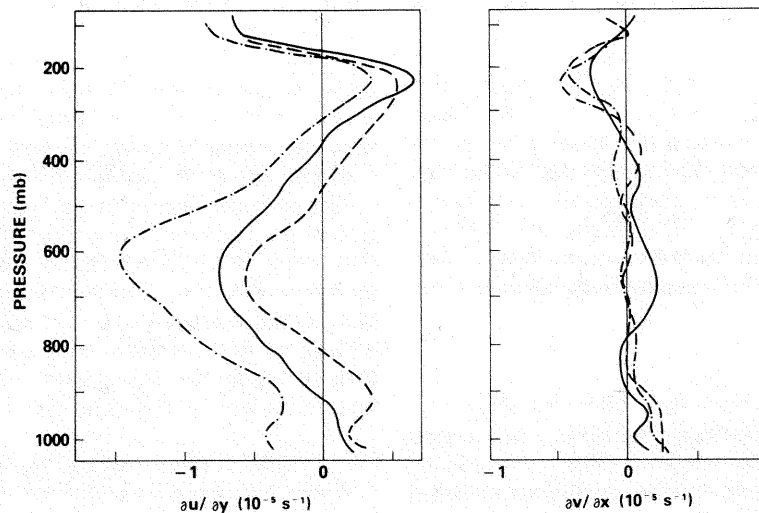


FIG. 3. Components of the relative vorticity  $\partial u/\partial y$  and  $\partial v/\partial x$ . Plotting convention same as in Fig. 2.

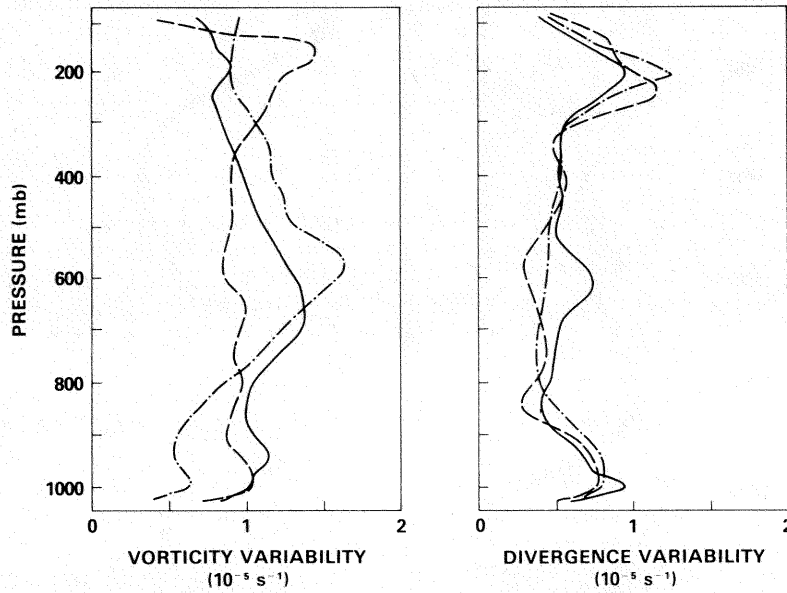


FIG. 4. Vorticity and divergence variability. Plotting convention same as in Fig. 2.

quantities of the vorticity budget, are formed by averaging the individual 12 h values.

The notation is as follows:

- $U, u$  zonal component of the wind
- $V, v$  meridional component of the wind
- $\sigma$  the standard deviations (variability)
- $\omega$  vertical velocity
- $\zeta$  relative vorticity
- $\beta$  latitudinal variation of Coriolis parameter,  $f$
- $\tau$  stress vector
- $\mathbf{V}_h$  horizontal wind vector
- TEJ Tropical Easterly Jet (upper troposphere wind maximum)

AEJ African Easterly Jet (middle troposphere wind maximum)

a. Phase-mean profiles

1) RELATIVE VORTICITY

The mean relative vorticity profiles (Fig. 2) are similar in shape for all three phases, and agree qualitatively with the Phase III profile shown in Thompson *et al.* (1979). However, the Phase I mean is more cyclonic throughout and is the only profile to show relatively large cyclonic vorticity in the boundary layer. Even though the circulation is more cyclonic

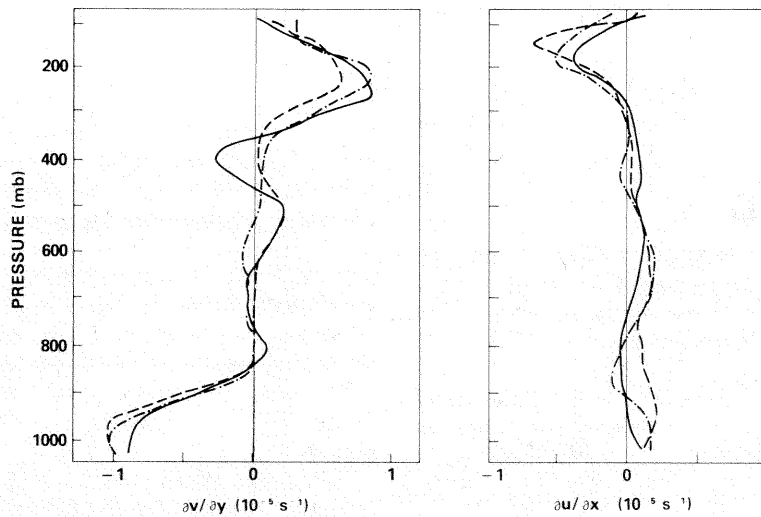


FIG. 5. Components of the divergence  $\partial u/\partial x$  and  $\partial v/\partial y$ . Plotting convention same as in Fig. 2.

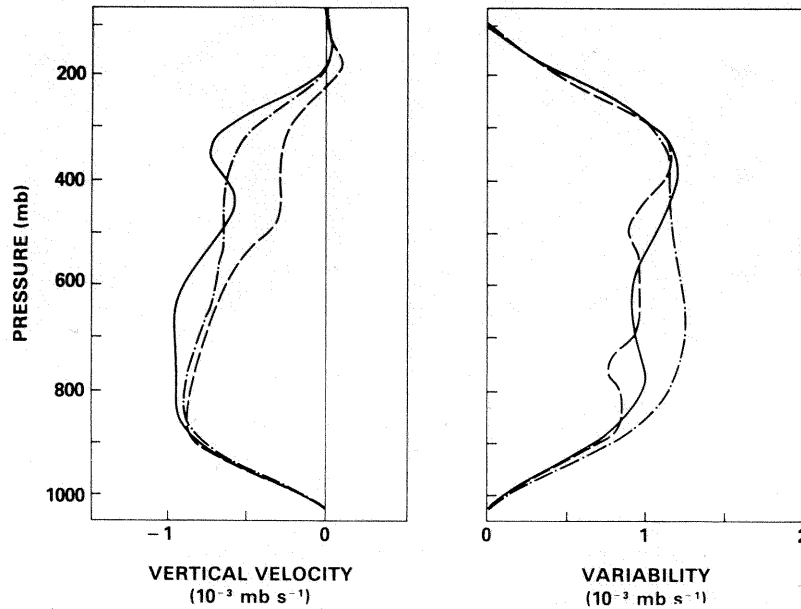


FIG. 6. Mean vertical velocity and variability. Plotting convention same as in Fig. 2.

during Phase I, the mean precipitation rate over the B array ( $0.49 \text{ mm h}^{-1}$ ) is not very different from that observed during Phase III ( $0.53 \text{ mm h}^{-1}$ ). Both amounts are greater than the mean precipitation rate during Phase II ( $0.38 \text{ mm h}^{-1}$ ). The latitudinal variation of the zonal wind component,  $-\partial u/\partial y$ , makes the main contribution to the vorticity (Fig. 3). The large cyclonic values of this term in the middle troposphere are a consequence of the position of the AEJ to the north of the array. The cyclonic shear is considerably weakened during Phases II and III. The TEJ, on the other hand, has its maximum over the array as indicated by the zero value of  $-\partial u/\partial y$  at the level of the jet. There is little systematic variation in the  $\partial v/\partial x$  vorticity component. The anticyclonic peak at 200 mb contributes to the strong anticyclonic peak on the mean vorticity profile.

The  $\sigma(\zeta)$  in Fig. 4 remains on the order of  $10^{-5} \text{ s}^{-1}$  for all three phases, with little systematic height variation.

## 2) VELOCITY DIVERGENCE

The mean divergence profiles (Fig. 2) and the individual profiles of  $\partial u/\partial x$  and  $\partial v/\partial y$  (Fig. 5) show only minor differences from phase to phase. The relatively strong boundary-layer convergence is in

TABLE 2. Vertical velocity at 100 mb. Mass balance not imposed.

Phase	$W$ ( $\text{mb s}^{-1}$ )	$W$ ( $\text{mb day}^{-1}$ )
I	$2.6 \times 10^{-4}$	23
II	$1.2 \times 10^{-4}$	10
III	$2.3 \times 10^{-4}$	20

qualitative agreement with profiles presented by Brummer (1978) and is a reflection of the latitudinal gradient of the meridional wind component  $\partial v/\partial y$ . This term may reflect the presence of the ITCZ in the observational array during most of the experiment. At higher levels ( $\sim 200 \text{ mb}$ ) the positive contribution to the divergence from  $\partial v/\partial y$  exceeds a negative contribution of  $\partial u/\partial x$  indicative of the deceleration of the TEJ. As with  $\sigma(\zeta)$ , the  $\sigma$  (div) profiles show little difference from phase to phase (Fig. 4). There is a weak maximum in variability in the vicinity of the TEJ.

## 3) VERTICAL VELOCITY

The Phase mean vertical velocity at 100 mb, without mass balance imposed (Table 2), is a measure of the errors in this computation. The values for all phases are less than  $25 \text{ mb day}^{-1}$ . The phase mean  $\omega$  profiles, Fig. 6, are similar in shape. Thompson *et al.* (1979) obtain a similar profile for the B array in Phase III. The mean vertical motion in the upper troposphere was weakest during Phase II, the Phase with the lowest average precipitation rate. The maximum upward vertical motion occurs in the lower troposphere during each phase, a consequence of strong convergence in the boundary layer and weak divergence in the middle troposphere.

The  $\sigma(\omega)$  values are of the same order as  $\omega$  and do not show systematic variations from phase to phase.

While the phase mean vertical velocity profiles are quite similar, the phase mean precipitation patterns, Hudlow (1977), are quite different. In Phase I, radar shows that the precipitation is concentrated

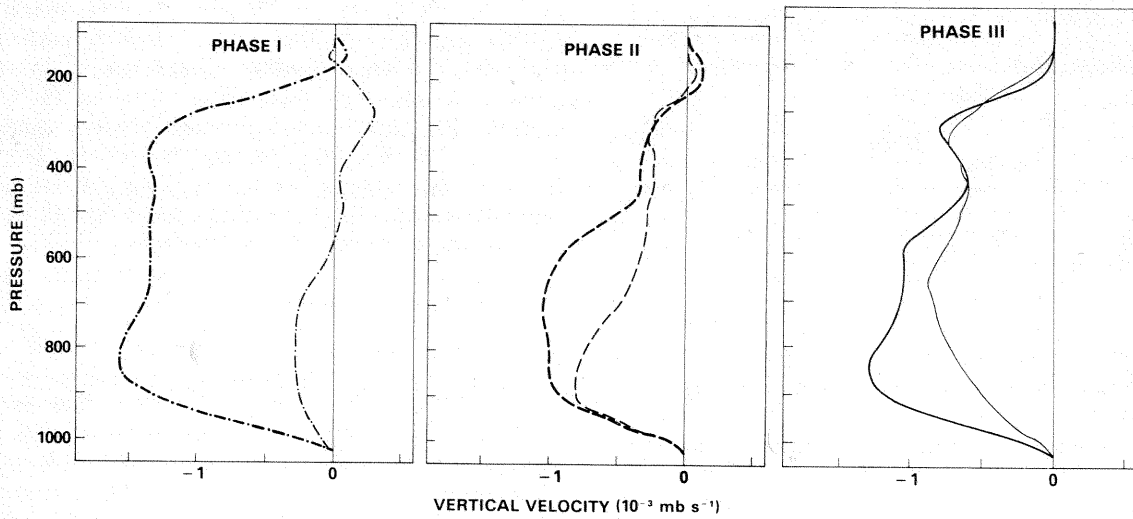


FIG. 7. Mean vertical velocity at 6.5°N (heavy) and 10.5°N (light).

in the southern half of the array. The raingages aboard the northernmost ships in the A/B array caught no precipitation, (Seguin and Sabol, 1976), while a considerable amount of rainfall was recorded over the center and southern portions of the array. A more uniform spatial distribution of precipitation was observed during Phases II and III. This pattern is reflected in values of  $\omega$  evaluated from the second-order fit of the wind components at points 2° latitude to the north and to the south of the center of the array (Fig. 7). In Phase I there are striking differences in the mean vertical velocity profiles for the southern (strong upward motion) and northern (weak downward motion) parts of the

array. The profiles for Phases II and III show a much more uniform mean vertical motion field. The vertical motion-precipitation rate relationship is explored further in the next section through a comparison for disturbed and suppressed conditions.

*b. Mean profiles for disturbed and suppressed conditions*

Radar estimates of the rainfall rate over the B array are used to distinguish between highly disturbed and suppressed conditions. For purposes of forming comparisons in this paper, highly disturbed periods are defined as those for which the 12 h average rain-

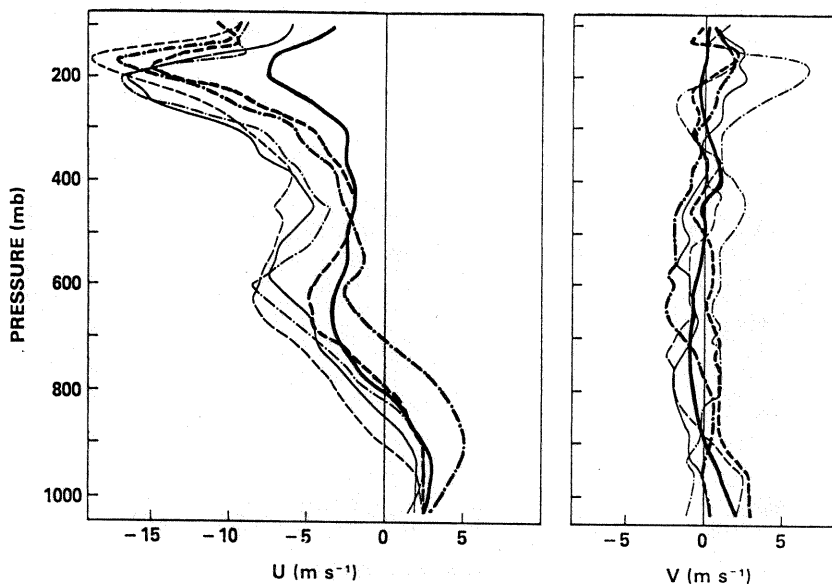


FIG. 8. Zonal and meridional wind profiles for disturbed (heavy) and undisturbed (light) for Phase I (dashed-dotted line), Phase II (dashed line), Phase III (solid line).

TABLE 3. Number of 12 h periods and the average precipitation rate in  $\text{mm h}^{-1}$  for the suppressed and disturbed composites.

	Suppressed		Disturbed	
	Number	Precipitation rate	Number	Precipitation rate
Phase I	14	0.03	15	1.04
Phase II	10	0.04	12	0.79
Phase III	4	0.02	16	1.04

fall rate over the B array is  $>0.5 \text{ mm h}^{-1}$ ; suppressed periods as those for which this average is  $<0.1 \text{ mm h}^{-1}$ . These threshold values were selected to provide as clear a separation between atmospheric states as possible and yet include a substantial amount of the data from the experiment. Periods during which the rainfall rates are  $>0.1 \text{ mm h}^{-1}$  but  $<0.5 \text{ mm h}^{-1}$  are not included in the analyses. Table 3 shows the number of cases in each category for each Phase and the average precipitation rate for each category. Although there are only four independent cases in the suppressed category in Phase III, the mean profiles are presented for completeness.

### 1) $U, V$ COMPONENTS

The profiles of the zonal wind, Fig. 8, reveal a more easterly flow through most of the troposphere during suppressed periods, with the AEJ stronger, and more sharply defined than during the disturbed events. There is no significant difference in the meridional wind component shown in Fig. 8 between disturbed and suppressed periods.

### 2) RELATIVE VORTICITY

The mean profiles of relative vorticity for the disturbed and suppressed cases show distinct differ-

ences for Phases II and III (Fig. 9). The disturbed profiles generally show cyclonic vorticity while the suppressed profiles exhibit anticyclonic vorticity at most levels. The distinction between the vorticity for disturbed and suppressed cases is sharpest near the 700 mb level during Phase III. During Phase II the contrast between disturbed and suppressed profiles is not as strong, while during Phase I, there are no systematic differences.

### 3) VERTICAL VELOCITY

The mean vertical velocity profiles for the disturbed periods (Fig. 10) show upward motion ( $\approx -1.5 \times 10^{-3} \text{ mb s}^{-1}$ ) in the region from 900 to 300 mb for all three phases. This contrasts sharply with the mean profiles for the suppressed periods which show weak downward motion ( $\approx 0.2 \times 10^{-3} \text{ mb s}^{-1}$ ) above 600 mb and weak upward motion only in the lower troposphere. The differences between the vertical velocity profiles for disturbed and suppressed conditions show that vertical velocity computed on this scale is a good indicator of phase average precipitation over the B array.

The mean vertical velocity profiles are clearly different during suppressed and highly disturbed conditions. On the other hand, the relative vorticity profiles do not fall neatly into two classes. In order to understand better the relationship of the precipitation events to the divergence, vorticity and vertical velocity, we compare the time series of these quantities at 700 mb with the time series of the B-array precipitation rate.

### c. Time series

The discussion of the time series of the kinematic quantities is limited to the surface and 700 mb. We

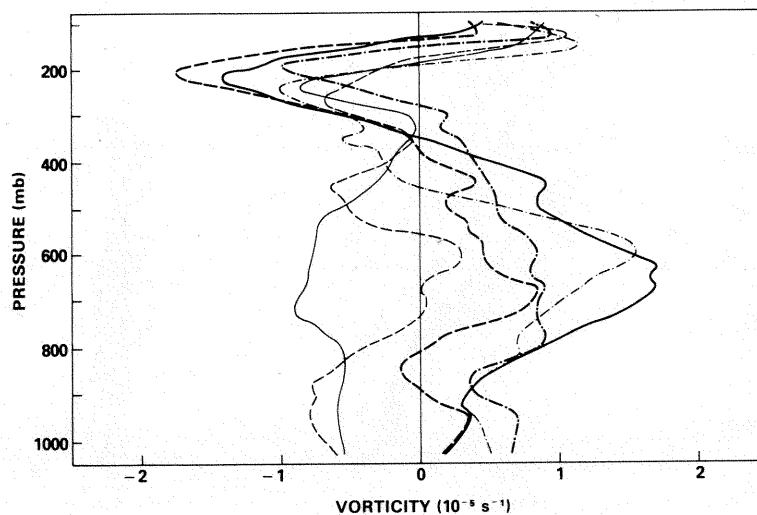


FIG. 9. Mean relative vorticity profiles for disturbed and suppressed conditions. Plotting convention same as in Fig. 8.

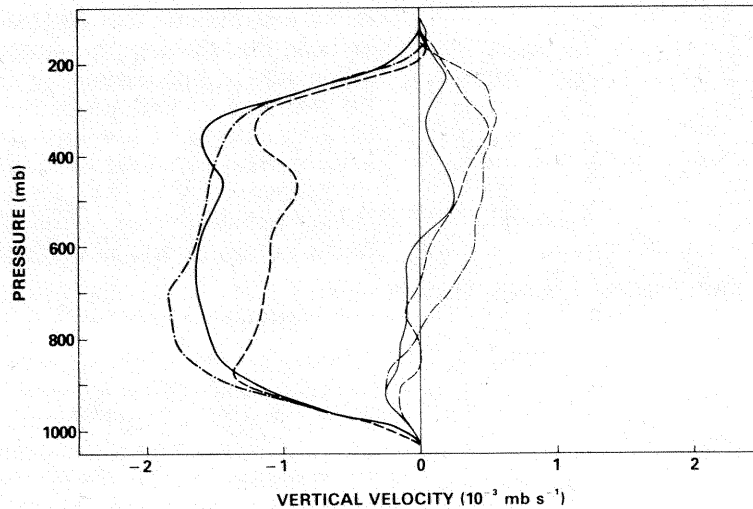


FIG. 10. Mean vertical velocity profiles for disturbed and suppressed conditions. Plotting convention same as in Fig. 8.

have chosen the latter because the amplitudes of the perturbations are particularly strong at 700 mb.

1) RELATIVE VORTICITY

The time series of 700 mb vorticity and precipitation rate in Fig. 11 reveals no obvious relationship between the two during Phase I and the first half of Phase II. However, during the latter half of Phase II and all of Phase III there is a close correspondence between the precipitation events and the peaks in cyclonic vorticity. This is in agreement with the Phase III findings of Reed *et al.* (1977), who attributed a significant part of the variations in vorticity and precipitation to the progression of easterly waves through the observational array. Some measure of the strength of the easterly waves is obtained

by inspection of Fig. 12, the time series of  $\partial v/\partial x$ , the component of vorticity which emphasizes the easterly waves. During Phases I and II, the behavior of  $\partial v/\partial x$  indicates that the waves are weaker and more poorly organized, in sharp contrast to Phase III where the peaks of precipitation correspond to the regular passage of wave troughs. The mechanisms for organizing the convection are apparently different for Phases I and II prompting examination of other kinematic quantities as common indicators of precipitation production.

2) VELOCITY DIVERGENCE

Recent studies have shown a positive relationship between surface convergence and precipitation on the mesoscale, e.g., Fernandez-Partagas

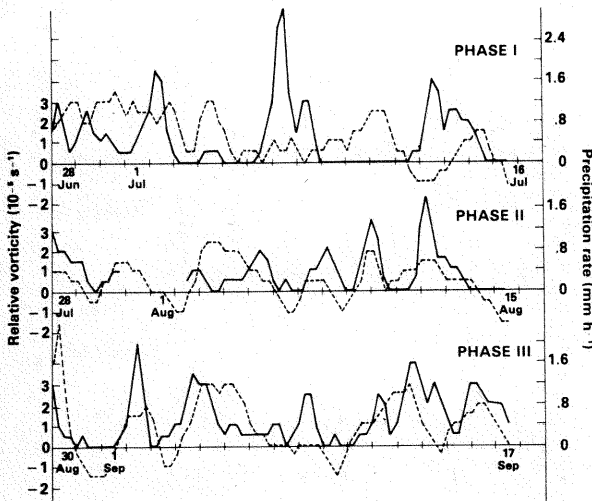


FIG. 11. Time series of 700 mb relative vorticity (dashed) and precipitation rate (solid).

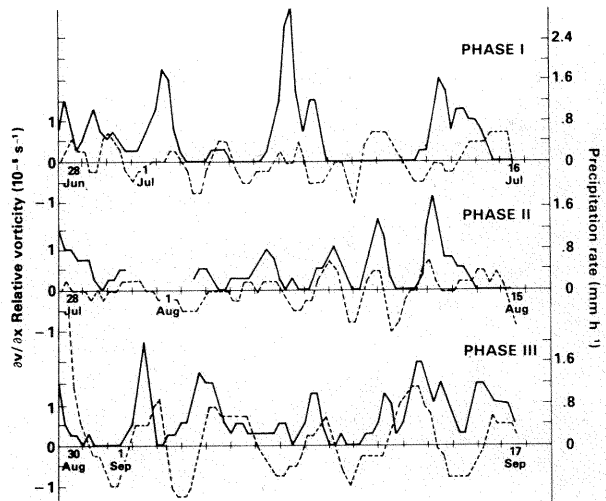


FIG. 12. Time series of 700 mb  $\partial v/\partial x$  vorticity contribution (dashed) and precipitation rate (solid).

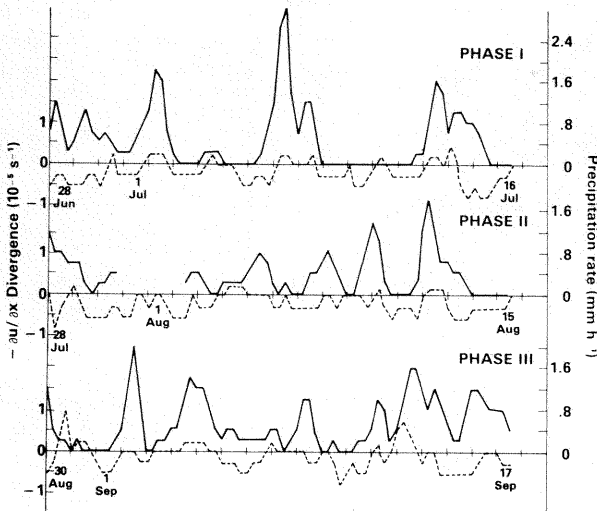


FIG. 13. Time series of surface  $\partial u/\partial x$  divergence contribution (dashed) and precipitation rate (solid).

(1973), Ropelewski and Reeves (1977), Ulanski and Garstang (1978), and Brummer (1978). Over the GATE area the surface flow was convergent 95% of the time. This is likely a reflection of the persistence of the ITCZ, which is confirmed by examination of the zonal ( $\partial u/\partial x$ ) and meridional ( $\partial v/\partial y$ ) components separately. The time series of  $\partial u/\partial x$  shown in Fig. 13 reveals the small divergent contribution from this component during all phases which does not appear to be related to the precipitation rate. On the other hand, the  $\partial v/\partial y$  term shown in Fig. 14 is relatively large and characterized by large-amplitude variations that may be a reflection of the strengthening and weakening of the meridional convergence typical of the ITCZ. The increases in

$\partial v/\partial y$  convergence are coincident with or slightly precede the increases in rainfall rate. The precipitation rate is then related to the strengthening of the meridional convergence rather than to the continued existence of low-level convergence. This is in agreement with a recent study over the C array by Brummer (1978). The apparent relationship of surface meridional convergence to the precipitation rate is present in all three Phases.

### 3) VERTICAL VELOCITY

Strong low-level convergence such as that manifest below 850 mb corresponds to upward vertical motion through a deeper layer.

(i) The A/B array. The relationship between the precipitation rate and 700 mb vertical velocity over the A/B array is examined in this section, and comparisons for two different horizontal scales represented by the A/B and B arrays are made in the following section.

Houze and Cheng (1977) found that most of the precipitation during GATE over the B array was associated with convective activity. One of the central questions of the experiment was whether the precipitation, due mainly to convection, could be parameterized with kinematic variables evaluated on much larger scales, e.g., the A/B array. The time series of vertical velocity, evaluated at 700 mb (Fig. 15), shows the close relationship between upward vertical motion at this level and precipitation over the master array. A clear relationship between upward vertical velocity and precipitation rate is evident even for those precipitation events which are poorly correlated with 700 mb vorticity or surface divergence. In some cases (e.g., 6–8 July, 13–14 September), complex variations in the pre-

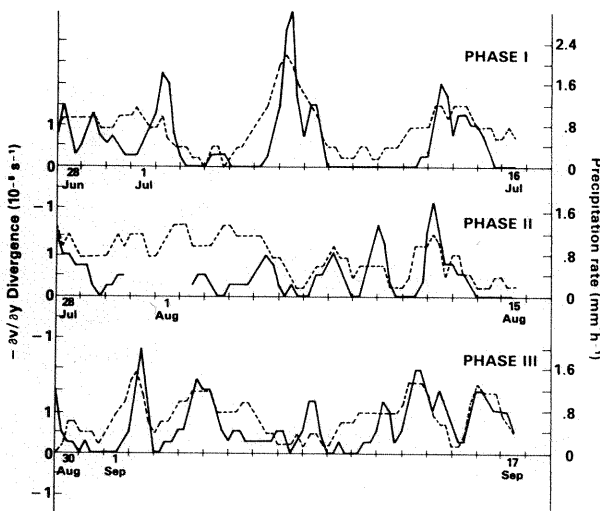


FIG. 14. Time series of surface  $\partial v/\partial y$  divergence contribution (dashed) and precipitation rate (solid).

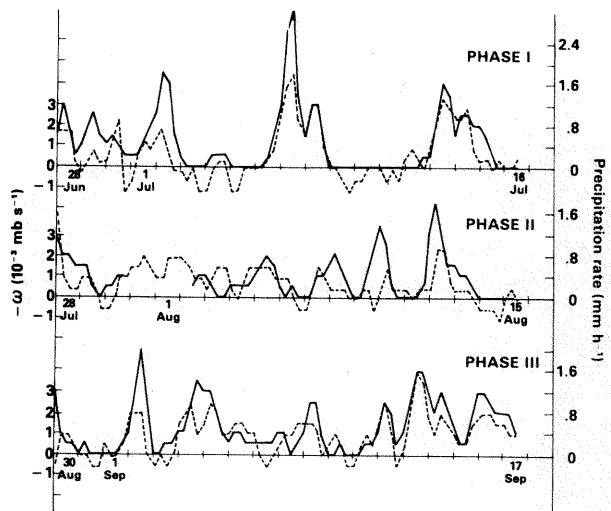


FIG. 15. Time series of 700 mb vertical velocity (dashed) and precipitation rate.

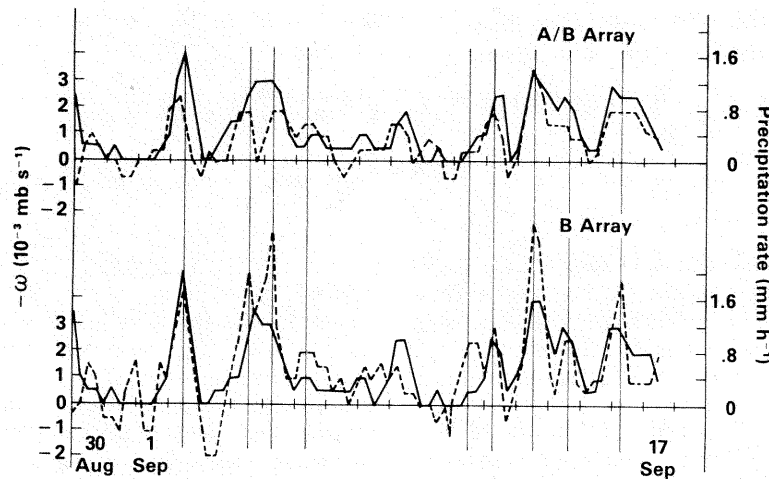


FIG. 16. Time series for Phase III of 700 mb vertical velocity (dashed) and precipitation rate (solid) for A/B and B arrays independently. Light vertical lines are drawn through the major upward vertical velocity peaks of the B array.

precipitation rate can be related to corresponding changes in the 700 mb vertical velocity. These time series then suggest that parameterization of convective precipitation in the numerical prediction models in the vicinity of the ITCZ may be feasible if reasonable estimates of the vertical velocity over scales comparable to the size of the A/B array can be obtained. Estimates of vertical motion over a few degrees of latitude could then be used to predict the integrated effects of convective-scale precipitation. Among the many models which utilize estimates of large scale vertical motion in the computation of precipitation are those of Kuo (1965), Manabe *et al.* (1965), and Arakawa and Schubert (1974).

(ii) Comparison between A/B and B array estimates. Some further measure of the relationship of vertical velocity and precipitation rate on different scales can be obtained through independent estimates of vertical velocity over the A/B and B arrays. This was done by computing, through a plane fit, the vertical velocity for the A/B array using data from the A/B ships only and for the B array using data from the B ships only. These estimates of vertical velocity over the A/B and B arrays are then compared to the precipitation rates over the master array and B array, respectively (Fig. 16). These independent estimates of the vertical velocity at the center of the arrays are consistent with each other and with the precipitation rates. The light vertical lines drawn through the upward vertical velocity maxima on the B array emphasize the strong simi-

larities between vertical motion time series on these two scales. These time series suggest that the vertical motion on the smaller scale, i.e., the size of the B array, is normally controlled by scales of motion at least as large as the A/B array. These results suggest that vertical velocity estimates on the larger A/B scale may be adequate for parameterization of precipitation over areas at least as small as the B array.

#### d. Vorticity budget computations

The results discussed in the previous section suggest a large-scale control on the degree or intensity of convective-scale activity. The feedback mechanism, i.e., the effects of the convective activity on the larger scale circulation, is examined through the vorticity budget. Computations of the vorticity budget by Riehl and Pearce (1968), Reed and Johnson (1974), Hodur and Fein (1977), Shapiro (1978) and Stevens (1979) revealed large imbalances when the terms of the equation were evaluated from the large-scale variables, which suggested the importance of these processes on scales smaller than the grid of observations. The imbalances have generally been attributed to the effects of cumulus convection. Since most of the precipitation during GATE was due to convective scale motion, we may obtain some idea of the effect of the smaller scale motions on the larger scale through a comparison of the vorticity budgets during suppressed and enhanced convective activity periods.

The vorticity equation in pressure coordinates is

$$\frac{\partial \zeta}{\partial t} + \mathbf{V}_h \cdot \nabla \zeta + \beta v + \omega \frac{\partial \zeta}{\partial p} = -(\zeta + f)(\nabla \cdot \mathbf{V}_h) - \mathbf{k} \cdot \nabla \omega \times \frac{\partial \mathbf{V}_h}{\partial p} - g \mathbf{k} \cdot \nabla \times \frac{\partial \boldsymbol{\tau}}{\partial p} \quad (1)$$

The sum of the terms on the left-hand side represents the total derivative of absolute vorticity. The first

term on the right-hand side is the divergence or production term, the second term is the tipping term, and the third is the friction term. Averaging over a horizontal area, indicated by an overbar, gives

$$\begin{aligned} \frac{\partial \bar{\zeta}}{\partial t} + \overline{\mathbf{V}_h \cdot \nabla \zeta} + \overline{\beta v} + \bar{\omega} \frac{\partial \bar{\zeta}}{\partial p} = & -\overline{(\zeta + f)(\nabla \cdot \mathbf{V}_h)} - \mathbf{k} \cdot \bar{\nabla} \omega \times \frac{\partial \overline{\mathbf{V}_h}}{\partial p} - \overline{g \mathbf{k} \cdot \nabla \times \frac{\partial \boldsymbol{\tau}}{\partial p}} \\ & - \overline{\omega' \frac{\partial \zeta'}{\partial p}} - \overline{\mathbf{V}_h' \cdot \nabla \zeta'} - \overline{(\zeta + f)'(\nabla \cdot \mathbf{V}_h)'} - \mathbf{k} \cdot \bar{\nabla} \omega' \times \frac{\partial \overline{\mathbf{V}_h'}}{\partial p}. \end{aligned} \quad (2)$$

The left-hand side and the first two terms on the right-hand side can, in principle, be evaluated directly from observations. The friction term and the mean products of the primed quantities cannot be evaluated directly, but their combined effect is estimated as a residual.

The vorticity budget profiles are shown in Figs. 17–21 with their  $2\sigma/\sqrt{N}$  confidence intervals. Averaging has been performed over 125 mb; thus to the extent that the individual 25 mb values that make up the layer averages are not randomly distributed uncorrelated variables, these errors are underestimated. On the other hand, to the extent that some portion of the variance is due to real meteorological variations, these error estimates are too large.

The mean divergence production term for the three Phases is shown in Fig. 17. The large and persistent boundary-layer convergence during GATE is responsible for the large mean values of positive vorticity production below about 800 mb. Anticyclonic vorticity production in the upper troposphere coincides with the mean divergence of upper levels.

The tipping term is difficult to evaluate, since it requires horizontal gradients of the vertical velocity. The term is often either ignored on the assumption that it is small, or included with the residual, and thus combined with subgrid scale processes. We

have evaluated the tipping term from the second-order fit and the results for each phase are shown in Fig. 18. The computed values of the term are comparable in magnitude to the divergence production term, with the major contribution from  $(\partial \omega / \partial y)(\partial u / \partial p)$ . Below about 400 mb the curves for the three phases are similar, with a peak of positive vorticity production between 700 and 800 mb. In the upper troposphere, however, strong differences occur between the three phases, from a cyclonic production peak in Phase I to virtually no production during Phases II and III. The major features of the profiles of the tipping term could be deduced, to some extent, from the mean zonal wind profiles for either suppressed or disturbed conditions shown in Fig. 10, and the vertical velocity profiles for 6.5 and 10.5°N for the three phases (Fig. 7). For example, the two strong production peaks in the tipping term for Phase I correspond to the two layers of easterly flow increasing between 700 and 600 mb and 400 and 200 mb, in the presence of a relatively strong north-south gradient of vertical velocity.

The vorticity budget residual appears in Fig. 19. The prominent feature common to all three Phases is the upper tropospheric cyclonic vorticity source. The pattern is more complicated than the one obtained by Hodur and Fein (1977) for a four-month

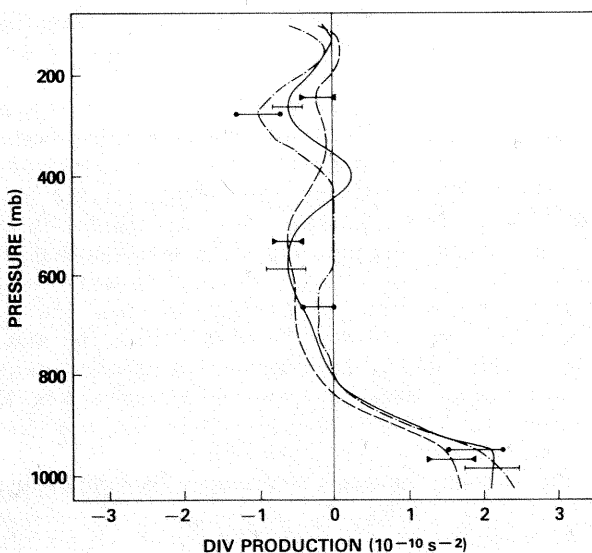


FIG. 17. Mean divergence production term for each Phase with  $2\sigma/\sqrt{N}$  confidence bands. Plotting convention same as in Fig. 2.

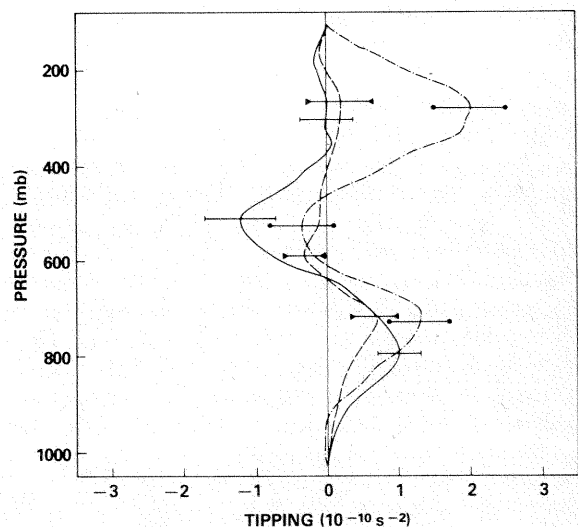


FIG. 18. Mean tipping term for each Phase with  $2\sigma/\sqrt{N}$  confidence bands. Plotting convention same as in Fig. 2.

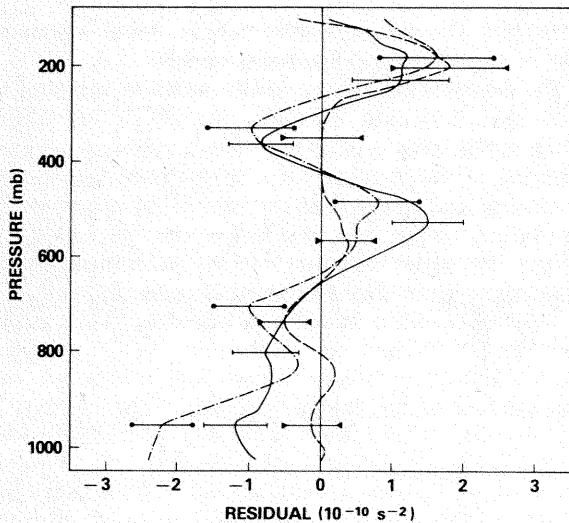


FIG. 19. Mean apparent vorticity source including friction and subgrid-scale processes only for each phase with  $2\sigma/\sqrt{N}$  confidence bands.

average in the region of the ITCZ in the Pacific. They obtained two maxima, an apparent cyclonic vorticity source in the upper troposphere and an anticyclonic source in the boundary layer. The upper tropospheric maximum for GATE is comparable in magnitude to the maximum of  $1.5 \times 10^{-10} \text{ s}^{-2}$  shown for Hodur and Fein's  $10^\circ \times 7^\circ$  grid domain.

While the mean vorticity budget profiles are similar for the three phases, there are interesting differences in disturbed and suppressed profiles. The production and tipping terms for the two states appear in Fig. 20. Strong differences occur in the production term, with boundary-layer cyclonic vorticity

production about four times as large for the disturbed cases. Large differences occur in the upper troposphere as well, with anticyclonic production during disturbed conditions and cyclonic production for the undisturbed periods. The cyclonic production aloft during suppressed periods is a reflection of the convergence associated with the weak upper tropospheric subsidence. There are no significant differences in the tipping term between disturbed and suppressed conditions.

The residuals for the two states are shown in Fig. 21. The similarity to the mean state of Fig. 19 can be seen. Two features are particularly significant: First, there is a definite tendency for more cyclonic subgrid-scale production in the mid-troposphere during the suppressed state; second, the apparent cyclonic vorticity source in the upper troposphere is equally strong during suppressed and disturbed states. The usual interpretation of the residual is that it represents the net effect on the large (or grid) scale by the smaller scale convective elements within the grid. This has been hypothesized by Riehl and Pearce (1968), Williams (1970), Holton and Colton (1972), and Reed and Johnson (1974). In the boundary layer, "friction" also accounts for a portion of the residual. The positive apparent vorticity source in the upper troposphere during suppressed conditions probably cannot be attributed to cumulonimbus activity, since it is not reasonable to expect significant or widespread deep convection with 12 h average B-array precipitation rates  $<0.1 \text{ mm h}^{-1}$ . Other vorticity budget studies have found large apparent vorticity sources in the upper troposphere under conditions of reduced convective activity. Stevens (1979), using data for Phase III of GATE, found an apparent cyclonic vorticity source in the upper

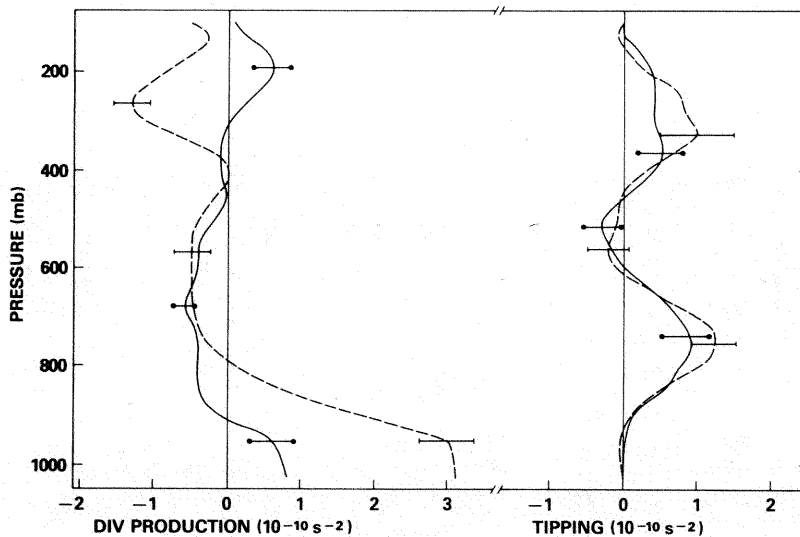


FIG. 20. Mean divergence production and tipping terms for disturbed (dashed) and suppressed (solid) conditions with  $2\sigma/\sqrt{N}$  confidence bands.

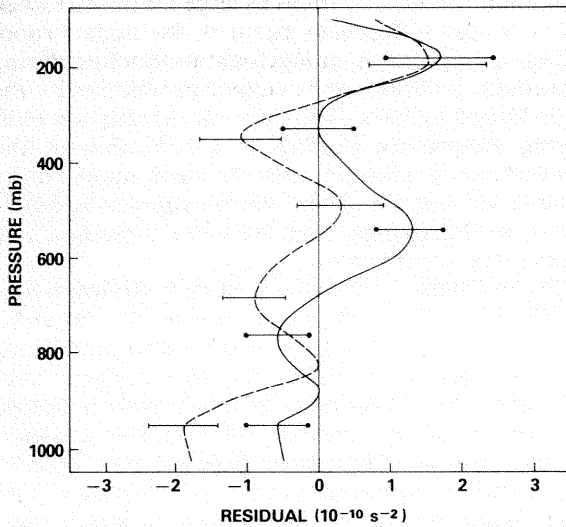


FIG. 21. Mean apparent vorticity source including friction and subgrid-scale processes only for disturbed (dashed) and suppressed (solid) conditions with  $2\sigma/\sqrt{N}$  confidence bands.

troposphere in the vicinity of a composite easterly wave ridge. He suggested the result may be due to uncertainties in the data. Fein (1977), in a global vorticity budget over the tropics, found areas with large magnitudes of the residual at 200 mb in regions of "minimal" convective activity. The vorticity budget residuals reported in those studies and in this study may be an artifact of the data due to either error in the rawinsonde winds or an inconsistency between temporal and spatial averaging scales. On the other hand, if we are to accept the residuals as meaningful, then physical mechanisms other than those associated with deep convection must be re-

sponsible for the apparent upper level vorticity source during suppressed conditions.

An explanation of the mean surface residual is facilitated, however, by consideration of the effects of the surface friction. If the surface stress is parameterized as the product of a drag coefficient times a velocity and speed then the curl of the stress in (2) can be expanded into two terms: one term that involves the cross product of the horizontal speed gradient and velocity and another term that reduces to a product of the speed and vorticity. Thus if the mean residuals near the surface in Fig. 21 are partially a reflection of the surface stress then we expect the surface residual to be related to the vorticity.

This is very often the case for both the suppressed (Fig. 22) and disturbed conditions (Fig. 23). A positive residual almost always occurs with a negative vorticity and vice versa. The mean negative surface residual during suppressed conditions is a reflection of the mean positive vorticity near the surface resulting from the predominance of cyclonic conditions during Phase I. If the residuals in the disturbed case represent mostly the effects of deep convection then their role under surface cyclonic conditions is almost always to reduce the magnitude of the surface vorticity.

#### 4. Summary and concluding remarks

The relationship of the precipitation to the mean winds on the scale of the GATE A/B array was examined by forming means for suppressed periods and periods of enhanced convection. We have related the vorticity, divergence and vertical velocity to the precipitation rate by comparing the time series

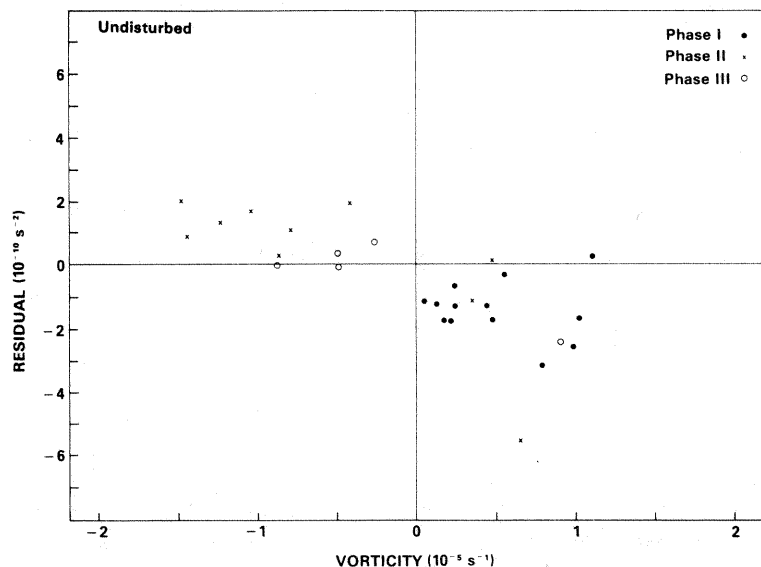


FIG. 22. Surface apparent vorticity source versus surface relative vorticity for suppressed conditions.

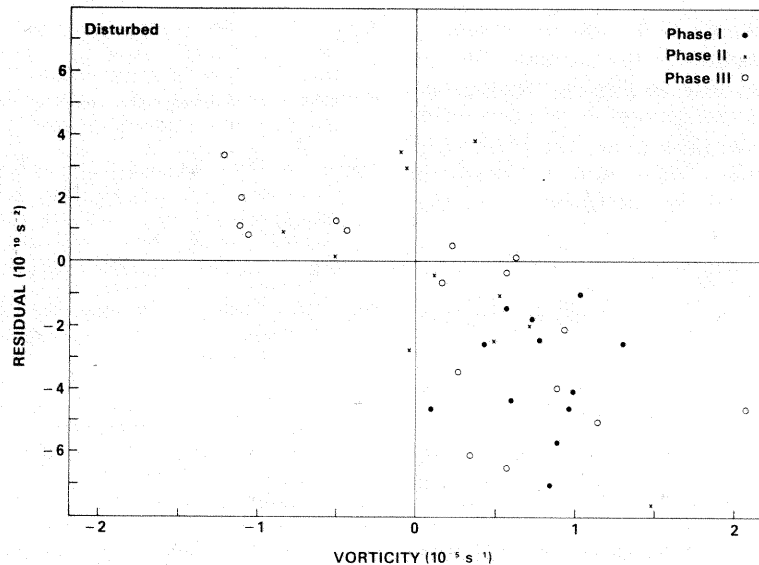


FIG. 23. As in Fig. 22 except for disturbed conditions.

of these kinematic variables at the surface and 700 mb to the precipitation time series. We have also attempted to evaluate the effects that the small scale, presumably associated with cumulus scale convection, have on the larger scale through our examination of the vorticity budget. The results of these analyses are summarized as follows:

1) Mean boundary-layer convergence balanced by upper tropospheric divergence results in mean upward vertical motion through most of the troposphere in all three phases. The mean upward vertical motion was weakest in the upper troposphere during Phase II, the phase with the lowest average precipitation rate.

2) During suppressed conditions, periods of very little convective activity, the mean vertical motion was weak upward in the lower troposphere and weak downward in the middle and upper troposphere. During highly disturbed periods, with enhanced convective activity, strong upward motion ( $>100$  mb  $\text{day}^{-1}$ ) existed in the mean over much of the troposphere.

3) During Phase III when the easterly waves were well-developed, the precipitation events corresponded very closely to the cyclonic peaks of the 700 mb relative vorticity. During Phases I and II, when the easterly waves were weaker and more poorly organized, the precipitation events did not correspond closely with the cyclonic vorticity maxima.

4) During all three phases, the precipitation events showed very good correspondence with the 700 mb upward vertical velocity maxima. Good correspondence was also observed between the

precipitation events and the surface meridional convergence  $\partial v/\partial y$ .

5) The tipping term for both suppressed and enhanced conditions appears to be important in the mean vorticity balance for the A/B array.

6) The vorticity budget residuals were similar from phase to phase, with maxima in cyclonic vorticity production in the mid and upper troposphere. Separation into mean suppressed and disturbed states revealed the unexpected result, that cyclonic vorticity production in the upper troposphere was as strong during the suppressed state as it was during the disturbed state. The residuals for the suppressed state may be a result of errors in the data, inconsistency of spatial and temporal averaging scales, or some physical mechanism other than that associated with deep convection.

7) The individual values of surface residual and surface vorticity were almost always opposite in sign. If the subgrid-scale production (i.e., the residual) during the disturbed state with cyclonic flow results largely from active convection, then the direct effect of the convection is almost always to reduce, not increase, the large-scale surface cyclonic vorticity.

8) Although most of the precipitation during GATE was of convective origin, this study has shown that it can be related to the large-scale (i.e., the size of the A/B array) vertical motion. If generally true, this suggests the feasibility of parameterizing the precipitation associated with the ITCZ by a numerical model with a relatively coarse ( $\sim 5^\circ$  of latitude) grid.

*Acknowledgments.* We wish to thank the GATE Project Office for providing the funding for this

study. John B. Jalickee's help was invaluable in formulating several aspects of the analysis. We express our appreciation also to Eugene Rasmusson for his encouragement and support during the course of this study. Carolyn Mackie typed the manuscript through several revisions. We extend our thanks to one of the reviewers for his comments and suggestions.

## REFERENCES

- Arakawa, A., and W. H. Schubert, 1974: Interaction of a cumulus cloud ensemble with the large-scale environment, Part I. *J. Atmos. Sci.*, **31**, 674-701.
- Burpee, R., 1975: Some features of synoptic-scale waves based on a compositing analysis of GATE data. *Mon. Wea. Rev.*, **103**, 921-925.
- Brunner, B., 1978: Mass and energy budgets of a 1 km high atmospheric box over the GATE C-scale triangle during undisturbed and disturbed weather conditions. *J. Atmos. Sci.*, **35**, 997-1011.
- Fein, J. S., 1977: Global vorticity budget over the tropics and subtropics at 200-mb during Northern Hemisphere summer. *Pure Appl. Geophys.*, **115**, 1493-1500.
- Fernandez-Partagas, J. J., 1973: Subsynchronous convergence-rain-fall relationship based upon 1971 South Florida data. NOAA Tech. Memo. ERL-WMPO-9, Boulder, CO, 76 pp.
- Hodur, R. M., and J. S. Fein, 1977: A vorticity budget over the Marshall Islands during the spring and summer months. *Mon. Wea. Rev.*, **105**, 1521-1526.
- Holton, J. R., and D. E. Colton, 1972: A diagnostic study of the vorticity balance at 200 mb in the tropics during the northern summer. *J. Atmos. Sci.*, **29**, 1124-1128.
- Houze, R. A., 1975: Squall lines observed in the vicinity of the *Researcher* during Phase III of GATE. *Preprints 16th Conf. Radar Meteorology*, Houston, Amer. Meteor. Soc., 206-209.
- , and C. P. Cheng, 1977: Radar characteristics of tropical convection observed during GATE: mean properties and trends over the Summer season. *Mon. Wea. Rev.*, **105**, 964-980.
- Hudlow, M. D., 1977: Precipitation climatology for the three phases of GATE. *Preprints Second Conf. Hydrometeorology*, Toronto, Amer. Meteor. Soc., 290-297.
- , and V. L. Patterson, 1979: *GATE Radar Rainfall Atlas*. NOAA Special Rep., Center for Environmental Assessment Services, 155 pp.
- , R. Arkell, V. Patterson, P. Pytlowany, F. Richards and S. Geotis, 1979: Calibration and intercomparison of the GATE C-band radars, NOAA Tech. Rep., Center for Environmental Assessment Services (in preparation).
- Jalickee, J. B., and W. J. Klepczynski, 1977: A method for compacting navigation tables. *Navigation: J. Inst. Navigation*, **24**, 125-131.
- Kuo, H. L., 1965: On formation and intensification of tropical cyclones through latent heat release by cumulus convection. *J. Atmos. Sci.*, **22**, 40-63.
- Manabe, S., J. Smagorinsky and R. F. Strickler, 1965: Simulated climatology of a general circulation model with a hydrologic cycle. *Mon. Wea. Rev.*, **93**, 769-798.
- Martin, D., 1975: Characteristics of West African and Atlantic cloud clusters based on satellite data. *WMO Global Atmospheric Research Program GATE Report*, No. 14, Preliminary Scientific Results, Vol. 1, 182-190.
- O'Brien, J. J., 1970: Alternate solutions to the classical vertical velocity problem. *J. Appl. Meteor.*, **9**, 197-203.
- Reed, R. J., and E. E. Recker, 1971: Structure and properties of synoptic-scale wave disturbances in the equatorial western Pacific. *J. Atmos. Sci.*, **28**, 1117-1133.
- , and R. H. Johnson, 1974: The vorticity budget of synoptic-scale wave disturbances in the tropical western Pacific. *J. Atmos. Sci.*, **31**, 1784-1790.
- , D. C. Norquist and E. E. Recker, 1977: The structure and properties of African wave disturbances as observed during Phase III of GATE. *Mon. Wea. Rev.*, **105**, 317-342.
- Reeves, R. W., 1978: GATE Convection Subprogram Data Center: Final report on rawinsonde data validation. NOAA Tech. Rep., EDS 29, 29 pp.
- Riehl, H., and R. P. Pearce, 1968: Studies on the interaction between synoptic and mesoscale weather elements in the tropics. Pap. No. 126, Dept. of Atmospheric Science, Colorado State University, 32 pp. [NTIS PB 185718.]
- Ropelewski, C. F., and R. W. Reeves, 1977: GATE Convection Subprogram Data Center: Comparison of ship-surface, rawinsonde and tethered sonde wind measurements. NOAA Tech. Rep. EDS 21, 22 pp. [NTIS PB-268-848.]
- Seguin, W. R., and P. Sabol, 1976: GATE Convection Subprogram Data Center: Shipboard precipitation data. NOAA Tech. Rep. EDS 18, 73 pp. [NTIS PB-263-820].
- Shapiro, L. J., 1978: The vorticity budget of a composite African tropical wave disturbance. *Mon. Wea. Rev.*, **106**, 806-817.
- Stevens, D. E., 1979: Vorticity, momentum, and divergence budgets of synoptic-scale wave disturbances in the tropical eastern Atlantic. *Mon. Wea. Rev.*, **107**, 535-550.
- Thompson, R. M., Jr., S. W. Payne, E. E. Recker and R. J. Reed, 1979: Structure and properties of synoptic-scale wave disturbances in the intertropical convergence zone of the eastern Atlantic. *J. Atmos. Sci.*, **36**, 53-72.
- Ullanski, S. L., and M. Garstang, 1978: The role of surface divergence and vorticity in the life cycle of convective rainfall, Part I: Observation and analysis. *J. Atmos. Sci.*, **35**, 1047-1062.
- Williams, K. T., 1970: A statistical analysis of satellite-observed trade wind cloud clusters in the western North Pacific. Rep. No. 161, Dept. of Atmospheric Science, Colorado State University, 80 pp.
- WMO, 1972: Experiment design proposal for the GARP Atlantic Tropical Experiment. GATE Rep., No. 1, WMO, 188 pp.